40 MHz Swept-Source Optical Coherence Tomography at 1060 nm Using a Time-Stretch and Supercontinuum Spectral Broadening Dynamics

Sacha Grelet, *Graduate Student Member, IEEE*, Alejandro Martínez Jiménez, Rasmus Dybbro Engelsholm, Patrick Bowen Montague, and Adrian Podoleanu

***Abstract*—We present an akinetically swept light source based on a spectrally broadened mode-locked laser in all normal dispersion optical fiber followed by a linear dispersive time stretch and a regenerative amplification stage. Developed for ultrafast swept-source optical coherence tomography (SS-OCT), the source enables the demonstration of A-scan rate at 40 MHz with a 12 μm axial resolution. Through A-scans captured from a fast-moving object, we demonstrate that high-speed OCT is possible at 1 μm wavelength in an architecture which is not intrinsically bandwidth limited. The source therefore shows a promising route to achieving high axial resolution in high-speed swept-source OCT.**

***Index Terms*—OCT, supercontinuum generation, fast imaging, swept source.**

I. Introduction

AMONG the ophthalmology community, optical coherence tomography (OCT) has become an indispensable tool that provides high-resolution three-dimensional images. A new challenge for OCT is to increase imaging speed in order to: 1) counteract motion artifacts, 2) create larger volume scans, while at the same time manifesting phase stability that can 3) add new functionalities such as OCT angiography (OCT-A) or optical coherence elastography (OCE) [1], [2], [3], [4]. Swept-source OCT (SS-OCT) uses a periodically tuned laser and a fast photodetector to reach high A-scan speeds, so far reaching tens of MHz [5], [6]. The quality and frame rate of images produced by SS-OCT is currently limited mainly by the light source characteristics, in particular, its spectral bandwidth, sweeping linearity, sweeping speed, and noise. The most used swept-sources for OCT employ microelectromechanical systems (MEMS) as mechanically controlled tunable spectral filters in Fourier domain mode-locking (FDML), or as one of the cavity mirror in MEMS vertical-external-cavity surface-emitting-laser (MEMS-VECSEL) [7], [8], [9]. Such devices produce unique results but appear to have fundamental limitation to their sweeping speed and/or bandwidth. An alternative to these sources is an akinetic swept source, where, in one implementation, a short broadband pulse is stretched in time, thereby leading to its different spectral components to be delivered at different instants [10], [11]. Numerous reports of such implementation exist in the telecommunication band, around 1550 nm, taking advantage of the low loss stretching elements based on silica fibers [12], [13], [14].

More than 50% of the reports on OCT refer to imaging the eye. While such systems could find immediate applications in the imaging of the anterior chamber of the eye, the large water attenuation renders the telecommunication wavelength too lossy for imaging the posterior chamber of the eye. Modern OCT systems for the posterior chamber use 800 nm and 1060 nm wavelengths, with recent preference for 1060 nm due to the more penetration depth in the choroid. Unfortunately, at this wavelength, low loss dispersive media do not exist whilst producing broadband (a few tens of nm) pulsed lasers requires complex cavity architecture [10], [15].

However, a new technology in supercontinuum has recently shown potential as it yields coherent, low-noise pulses which are spectrally flat and smooth.

This technology is based on the all-normal dispersion (ANDi) supercontinuum process, where a high peak-power femtosecond (fs) pulse propagates through a medium with normal dispersion and high nonlinearity. This form of supercontinuum generation is based on two coherent broadening mechanisms: self-phase modulation (SPM) and coherent optical wave-breaking (OWB), which together deliver a smooth, flat spectrum which is ideal for SS-OCT and, unlike typical supercontinuum, do not accrue additional noise in the process [16], [17], [18], [19], [20]. This is unique in supercontinuum-based OCT, and unlike previous demonstrations of spectrometer-based OCT configurations using ANDi supercontinuum, time stretched based swept source allows imaging at much faster rates, as determined by the inverse of the time stretch delay. For each laser pulse launched into the stretching element, an A-scan is produced.

Manuscript received 28 September 2022; revised 17 November 2022; accepted 30 November 2022. Date of publication 5 December 2022; date of current version 20 December 2022. The work was supported by the European Union's Horizon 2020 research and innovation programme under the Marie Skłodowska-Curie grant agreement No 860807. The work of Adrian Podoleanu was supported by the UCL Institute of Ophtalmology - Moorfields Eye Hospital under Grant BRC003. *(Corresponding author: Sacha Grelet.)*

Sacha Grelet is with the School of Physical Sciences, University of Kent, CT2 7NH Canterbury, U.K., and also with the NKT Photonics, 3460 Birkerød, Denmark (e-mail: sodg2@kent.ac.uk).

Alejandro Martínez Jiménez and Adrian Podoleanu are with the School of Physical Sciences, University of Kent CT2 7NH Canterbury, U.K. (e-mail: alejandromarjim@gmail.com).

Rasmus Dybbro Engelsholm and Patrick Bowen Montague are with NKT Photonics, 3460 Birkerød, Denmark (e-mail: rasmus.dybbro.engelsholm@nktphotonics.com; patrick.bowen.montague@nktphotonics.com; a.g.h.podoleanu@kent.ac.uk).

Digital Object Identifier 10.1109/JPHOT.2022.3226820

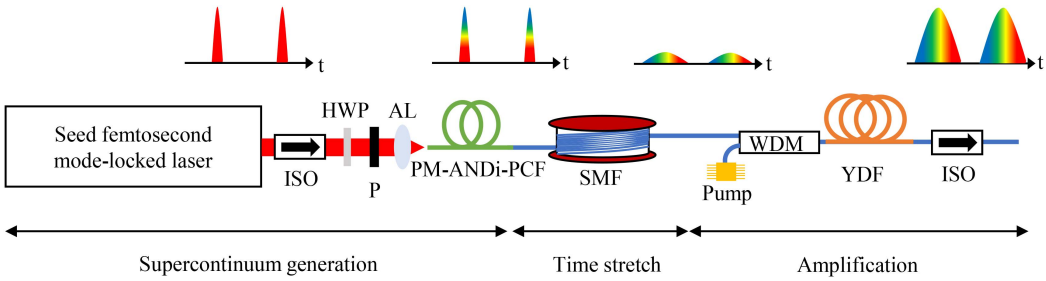

Fig. 1. Schematic of the swept-source and depiction of pulse evolution throughout the system. ISO, isolator; HWP, half-wave plate; P, polarizer; AL, aspheric lens; SM, single mode fiber; WDM, wavelength division multiplexer; YDF, Ytterbium doped fiber.

In this paper, we present a swept-source that utilises ANDi supercontinuum dynamics and fiber-based time stretching as a proof of concept, that achieves wavelength sweeping over a 48 nm bandwidth centered at 1060 nm at a 40 MHz rate. While the final OCT images in this paper have limited axial range, resolution, and sensitivity, the work nonetheless demonstrates the potential of ANDi supercontinuum processes to yield a light source for SS-OCT that can achieve sweeping rates of up to tens of MHz and a spectral bandwidth of hundreds of nm [21]. We further aim to show that the implementation of a swept source as described has the potential in a high average power after stretching, rendering no need for optical amplification, that may limit the final bandwidth delivered to the OCT interferometer.

II. 40 MHz Swept Source Development

The full swept-source setup is presented in Fig. 1. For the generation of the ANDi supercontinuum, a commercial fs ytterbium solid-state mode-locked laser (Origami 10 LP, NKT Photonics), centered at 1030 nm is employed. This laser produces 180 fs pulses at a 40 MHz repetition rate with an average power of 70 mW. It is designed to have a low RIN $<1\%$ and a polarization extinction ratio (PER) >24 dB. An isolator prevents feedback and the polarization of the light is aligned to the fast axis of the nonlinear fiber using a half-wave plate and a linear polarizer. An aspheric lens with 4.51 mm focal length is used to couple the light into the fiber. Due to component and coupling losses, 40 mW average power is coupled into the fiber which correspond to 2.45 kW peak power. A polarization-maintaining (PM) ANDi photonic crystal fiber (PCF) of 2.8 m length is employed (NL-1050-NEG-1-PM, NKT Photonics). The fiber needs to be PM to avoid noise from polarised modulation instability (PMI) [22]. The fiber core diameter is 2.4 μm, with a hole to hole pitch $\Lambda = 1.44$ μm, a relative hole diameter $\mathrm{d}/\Lambda = 0.39$ and a nonlinear coefficient $\gamma = 26.8$ $\mathrm{W^{-1}km^{-1}}$. The dispersion, D, has a parabolic profile with a maximum of -13 ps/km/nm at 1040 nm for propagation along the fast axis of the fiber [21], [22], [23].

The optimization of the fiber length for the supercontinuum generation was done using a numerical simulation based on the generalized nonlinear Schrodinger equation (GNLSE) [23], [24], [25]. The result of the simulations and the experimentally measured spectra are presented in Fig. 2. In the initial 25 cm of the fiber, the dominant nonlinear effect is SPM broadening.

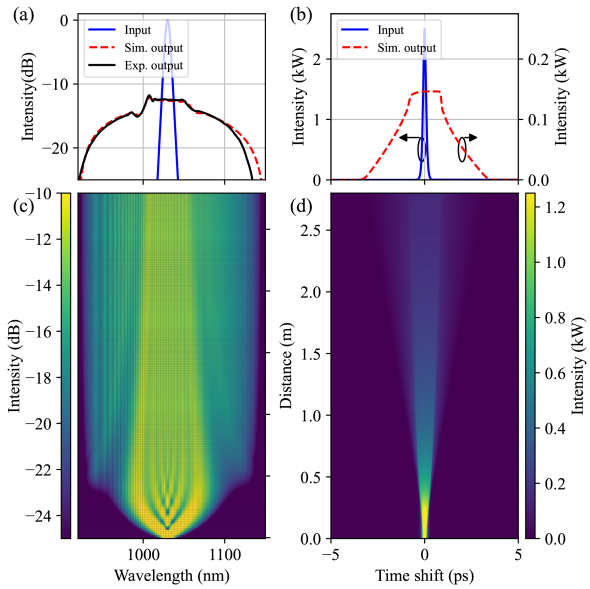

Fig. 2. ANDi supercontinuum generation. Simulation input (blue), simulation output (red dashes) and experimental output (black). (a) Spectral domain. (b) Time domain. (c)–(d) Evolution of the pulse in spectral domain and time domain during propagation.

Then, the OWB extends the spectrum further, first on the short wavelength side, then on the longer wavelength side. After pulse propagation though 75 cm of fiber, the spectrum is fully broadened. During the remaining length of the fiber, the effect of the normal dispersion and optical wave-breaking flattens and smoothens the spectrum, while further distributing energy to the spectral edges thereby giving a steepened spectrum that, once time-stretched, will have a shorter rise time. The spectrum measured is in good agreement with the simulation, with 100 nm bandwidth at full width half maximum (FWHM) and 200 nm bandwidth at -10 dB, centered at 1030 nm. The combination of the peak power in the input pulse and the material properties of the nonlinear fiber set the bandwidth and spectral power density. This has two significant implications. First, increasing the input laser power to the nonlinear fiber will increase the bandwidth. Earlier publications have yielded a smooth and flat spectra that already covered more than 700 nm bandwidths (at FWHM) [21]. This far exceeds the current bandwidth requirements for ultra-high axial resolution even in spectrometer-based OCT. Second, since the bandwidth is enlarged, increasing the input power to the

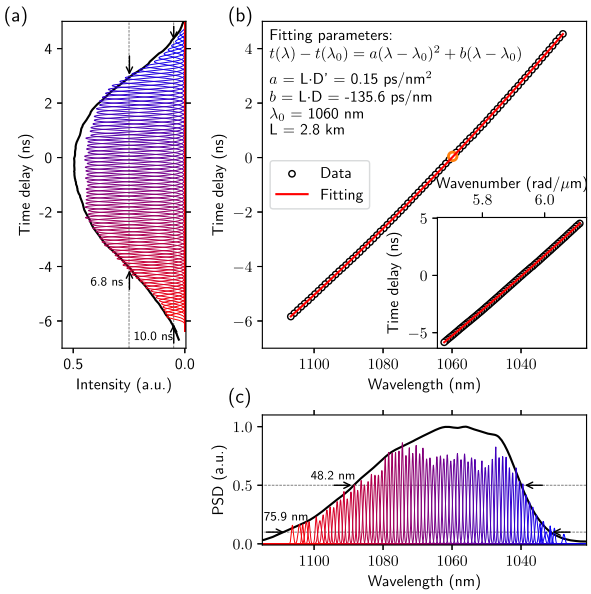

Fig. 3. Time warp measurement. (a), Time domain measurement. (c), Spectral domain measurement. Each position of the grating is presented with the same color in both domains. The black line corresponds to the pulse measured before the monochromator. The pulse duration and spectral bandwidth are measured at −3 dB and −10 dB. (b), Time warp fitted with a second order polynomial according to the formula presented. The inset presents the time warp in wavenumber with a second order polynomial fit.

nonlinear fiber negligibly increases the power spectral density (PSD). By selecting a new optical fiber that provides weaker nonlinear broadening, higher PSD can be achieved for the same bandwidth. In compromise for our currently available ANDi fiber, we later describe use of a ytterbium-doped fiber amplifier to regenerate the signal after stretching loss (see Fig. 1).

Pulse time-stretching, or dispersive Fourier transformation (DFT), is the process of propagating a near-transform-limited, broadband pulse through a medium that induces a large group velocity dispersion (GVD). The spectrum is mapped into the time domain and, if the dispersion is known, the spectrum of the pulse can be determined precisely by using a fast photodiode and precisely synchronized digitizer.

The most commonly used dispersion device is a long single-mode fiber (SMF), here 2.7 km of Nufern 980-XP. With a fiber loss of 3 dB/km and a dispersion of −48.4 ps/nm/km at 1060 nm, the 100 nm bandwidth could be stretched from 2 ps to 13.5 ns suffering a power loss to 2.9 mW. This choice of fiber length was planned to achieve a high duty cycle using a seed laser at 80 MHz, though we note a 40 MHz source was available for the experiment. In order to retrieve nominally useful images with the available OCT imaging system, the swept source required amplification to 20 mW. Therefore, an ytterbium-doped fiber amplifier is appended to increase the output power to 22 mW. However, the narrow bandwidth of the gain medium reduces the output spectral bandwidth to 48.2 nm at FWHM and to 75.9 nm at −10 dB centered at 1060 nm, as it can be seen in the dispersion mapping in Fig. 3(c). This ultimately limits the axial resolution of the OCT using this source. With the limited bandwidth, the pulse duration is also reduced to 10 ns at −10 dB, as shown in Fig. 3(a).

The time domain to spectral domain mapping of the frequency sweep, called a time warp [26], is an important parameter for the OCT processing, as it is necessary to correctly relate time measurements to frequency. To measure the time warps, a set-up is used in which the light is collimated and injected into a monochromator (SpectraPro 2300i by Princeton Instruments). The light passes through this broadband tunable filter and is measured in the time domain using a 5 GHz InGaAs photodiode terminated on a 12 GHz sampling oscilloscope (PicoScope 9200). The arrival time is then referenced by the electrical trigger output of the seed laser, and concurrently, the spectrum is measured on an optical spectrum analyser (OSA) using an integrating sphere and a multi-mode fiber pick-up. In Fig. 3, each peak is fitted with a gaussian function, and the relative time delay Δt against the corresponding central wavelength is extracted. The mapping is then converted from wavelength to wavenumber.

As presented by the fit in Fig. 3, the minimal amount of higher-order dispersion, represented by $L \cdot D' = L \cdot dD/d\lambda = L \cdot 2\pi/k_0^2 \cdot (-dD/dk)$, eases the requirement for compensation of the sweep nonlinearity during the OCT processing. This is a general advantage for fiber based stretching as it applies linear wavenumber dispersive delay which is often approximated by a complex filter driving waveform in an active filter based approach [27].

Finally, as the seed laser has a low relative intensity noise (RIN), the spectrum after broadening is very stable both in amplitude and bandwidth [16], [18], [19], [20]. For this reason, using a passive stretching device like the one presented delivers a temporally stable sweeping where all the pulses are the same. This lifts the need for precise pulse to pulse synchronization for the OCT application.

III. High Speed SS-OCT Imaging

The time-stretched swept-source signal is then injected into a symmetric optical fiber interferometer, presented in Fig. 4. The signal propagates through an array made of three identical 50/50 couplers with matched fiber lengths, where it is divided into a reference and a sample arm. In the reference arm, the light is collimated and reflected on a mirror placed on a translation stage to create a variable optical delay line (VODL). In the sample arm, the light is first collimated, and then focused on the sample. The power in both arm is ∼2.8 mW. The interference pattern is detected by a 23 GHz balanced photodetector (BPR-23-M by Optilab). Due to losses in the symmetric array, measured to be 4 dB and probably due to connectors and internal splices, the power at each input of the photodetector is 0.55 mW. The electric signal is digitized by an 80 GS/s, 20 GHz, 8 b oscilloscope (WaveMaster 820Zi-B by Teledyne Lecroy) and collected by a computer for processing. An in-line fiber polarization controller allows modification of the polarization in the sample arm to match the polarization in the reference arm. The oscilloscope is triggered by the 40 MHz seed.

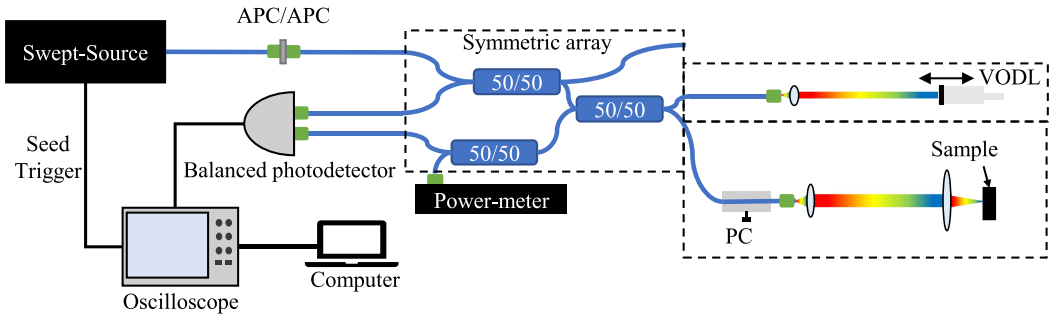

Fig. 4. Experimental set-up of the OCT system. APC, angled polished physical contact fiber connectors; PC, polarization controller; VODL, variable optical delay line.

Complex master-slave (CMS) OCT, extensively described in [28], [29], was used to reconstruct the depth information. In this method, a photodetected signal acquired during a sweep is compared to a set of functions (masks), where each mask is a channeled spectrum containing only a single reflection at various depths. Specifically, 10 channeled spectra were acquired in advance, using a mirror as sample set at 10 different optical path differences (OPD) within the axial range of the OCT imaging system. This initial set was subsequently used to generate a complete set of 10,000 synthesized masks covering all the axial range [28], [29]. After the calibration, the mirror is replaced with the sample and the channelled spectra obtained are processed by the CMS algorithm. This can be described by a product between a matrix M containing the masks and the vector I containing the channeled spectrum:

$$\begin{bmatrix} A(z_1) \\ \vdots \\ A(z_N) \end{bmatrix} = \begin{bmatrix} M^*(t_1, z_1) & \dots & M^*(t_\tau, z_1) \\ & \vdots & \\ M^*(t_1, z_N) & \dots & M^*(t_\tau, z_N) \end{bmatrix} \cdot \begin{bmatrix} I(t_1) \\ \vdots \\ I_(t_\tau) \end{bmatrix} \quad (1)$$

with $A(z)$ the CMS-OCT signal corresponding to the depth z, N the number of synthesized masks and τ the number of sampled points, which depends on the sampling rate of the oscilloscope. It should be noted that in the experiment later described, the amount of data makes real time transfer to a processing unit impossible. The data is first stored in the oscilloscope and then transferred to a computer for processing. In this situation, CMS processing presents similar performance with Fourier transform processing [29].

The system characterization, presented in Fig. 5, is performed using a single reflective interface at the sample position. A Hamming function is used for apodization on the generated masks. An axial resolution in air of 12 μm is obtained which is close to the 10.3 μm limit imposed by a 48.2 nm wide spectrum.

Due to high loss throughout the system, the photodiode was not saturated, meaning that the signal to noise ratio (SNR) measured corresponds to the system sensitivity. To elaborate on this, we consider the possible noise contributions in terms of shot noise, detector noise, and excess photon noise [30]. Until now, most reports of OCT sensitivity at multi-MHz scan rates consider the shot noise as the limiting parameter [6], [7]. Based on the same assumption, we calculate the maximum sensitivity in our system to be 72 dB. In comparison to OCT systems operating at hundreds of kHz to MHz sweep rates, which typically have

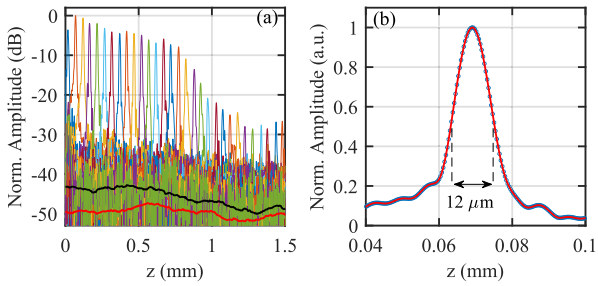

Fig. 5. OCT system characterization. (a) A-scans for different OPD values. The bottom black and red lines are respectively measurements of the system noise floor and the detector noise. (b) A single A-scan showing an axial resolution at FWHM of 12 μm in air.

a shot-noise limited sensitivity higher than 90 dB, the short integration time due to high speed imaging clearly poses a significant barrier.

By measuring the noise present on the balanced detector when no optical power is applied, we determine the receiver noise to be 51 dB, as shown by the red line in Fig. 5(a). When applying the optical power, the noise floor raises to 41 dB shown by the black line in Fig. 5(a), indicating that receiver noise is not the dominating noise contribution. This value, less than 72 dB, also confirms that the system is not shot noise limited.

Therefore, the excess photon noise is studied, specifically considering the relative intensity noise (RIN). To perform this measurement, 1000 consecutive channeled spectra have been acquired using a mirror as a sample, then transferred from time domain to spectral domain via the time warp presented in Fig. 3, and the envelope of each channeled spectrum is obtained. Using these envelopes, the RIN is then calculated for each spectral point as:

$$RIN(\lambda) = \sqrt{\langle(|\hat{A}(\lambda)|^2 - \langle|\hat{A}(\lambda)|^2\rangle)^2\rangle}/\langle|\hat{A}(\lambda)|^2\rangle \quad (2)$$

Fig. 6 shows that, similar to ANDi supercontinuum reported in our previous work [21], a low RIN $\sim 3-4\%$ is obtained across the FWHM bandwidth. This value is significantly lower in comparison to $\sim 20\%$ measured in OCT reports using anomalous-dispersion-supercontinuum dynamics [18]. The RIN spectrum does not show characteristics of incoherent broadening mechanisms induced by Raman scattering, technical noise, or polarization modulation instability [16], [22]. It is therefore characteristic of low-noise ANDi supercontinuum dynamics,

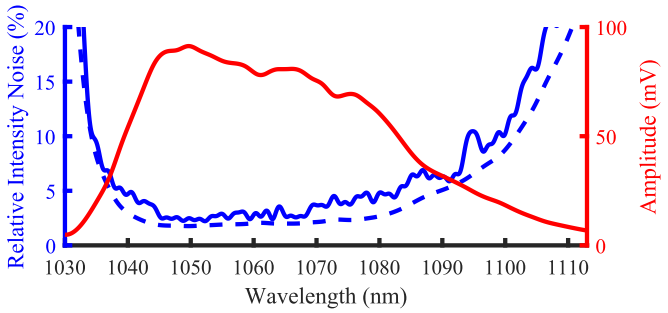

Fig. 6. RIN system characterization. Experimentally measured relative intensity noise (in blue) for 1000 consecutive channeled spectra with the detector limit (dotted blue), and the averaged channel spectrum envelope (red).

confirming that both the seed laser and nonlinear broadening process are low noise. We therefore attribute the 41 dB sensitivity to excess noise generated by amplified spontaneous emission in the amplifier [13] and minor wavelength-dependent imbalance on the couplers which leads to inefficient cancellation of noise at the balanced detection output. We specifically note that noise from amplified spontaneous emission in the amplifier is an incoherent noise source that cannot be eliminated by balanced detection [31]. To improve this sensitivity in future trials, two main considerations should be made. First, the use of an amplifier could be avoided by employing a higher power seed and/or a less lossy stretching mechanism, for instance, a chirped fiber Bragg grating. Second, more power from the sample would be required on the balanced detector. This could be achieved by reducing interferometer losses and using an asymmetric design, by increasing source power. Another possibility would be to stretch the pulses up to the seed laser period which leads to reduction in the electrical bandwidth needed, consequently reducing the noise.

A roll-off of the amplitude of -9 dB/mm has been measured, with a -6 dB value at 0.67 mm. A theoretical roll-off at -6 dB is calculated as:

$$z_{-6\,dB} = \frac{\ln(2)}{\pi} \cdot \frac{\lambda_0^2}{\delta\lambda} \tag{3}$$

where λ_0 is the central wavelength, $\delta\lambda$ is the spectral linewidth calculated as $\delta\lambda = 1/(|D|L \cdot B_{scope})$, with $|D|L$ the dispersion in the time stretch (respectively the fiber dispersion and length), the sampling rate B_{scope} [32], [33]. A spectral linewidth of 0.369 nm is obtained, leading to a theoretical roll-off at -6 dB of 0.672 mm, which agrees with the experimental result.

To illustrate the capability of fast imaging enabled by the fast sweeping rate, a rotating chopper is used to scan the sample on the stationary laser beam. A representation of the sample, prepared on the chopper, is presented in Fig. 7(a). First, one layer of optical tape covers the chopper: composed of a 25 μm polyimide backing film and a 45 μm silicone adhesive layer. On top of the optical tape, small pieces of Crystal tape are placed (by Scotch, thickness of 42 μm $\pm$ 1 μm independently measured using an high resolution OCT). These two sample are used to demonstrate OCT imaging on fast moving scattering multi-layered phantoms. Finally, a metallic wire, whose diameter is measured to be 70 μm is placed perpendicular to the rotation direction. This last object is used to demonstrate the resolving capabilities of the high speed

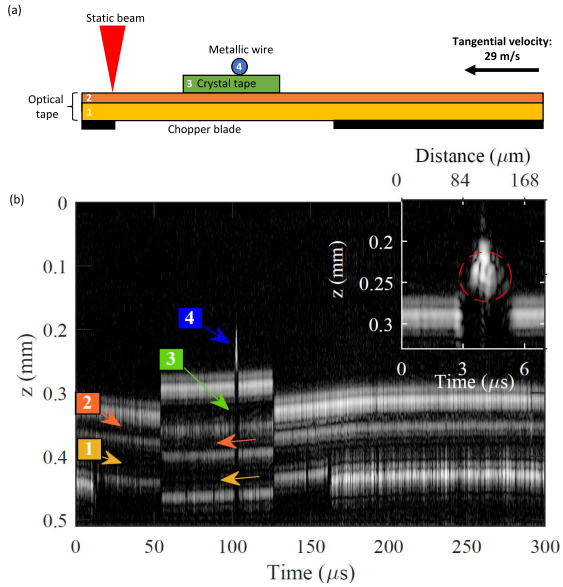

Fig. 7. Imaging of fast moving objects. (a) Representation of the sample used. Several objects are imaged: 1 Adhesive layer and 2 backing film of an optical tape covering the whole surface of a rotating chopper disk, 3. Short piece of Crystal tape, 4. 70 μm metallic wire. (b) OCT image. The insert is a zoom on the area 4. A circle in red dots with a 70 μm diameter is plotted for scale.

system. With the chopper rotating at 110 Hz and the probing beam incident on the chopper at 4.2 cm from its rotational axis, a tangential speed of 29 m/s was reached. As the A-scan rate is equal to the pulse rate (40 MHz), the apparent scan rate of 0.7 μm per A-scan was observed. With a transverse resolution of 10 μm, we note that faster scanning speeds achievable with a resonant scanner or KTN crystal would be preferable.

Fig. 7(b) shows 12,000 consecutive A-scans recorded in 0.3 ms. In the first and second areas, respectively marked by yellow and orange arrows, the optical tape is recognizable by the 3 interfaces between the air, the adhesive layer (1), the backing film (2) and air. The respective thickness of both layers is measured to be 69 μm and 40 μm. This matches the expected equivalent distance in air (calculated to be 61 μm and 43 μm) that takes into account the refractive index of these materials. In the third area marked by the green arrow, one small piece of Crystal tape is measured, with a thickness of 67 μm (66 μm calculated). The high speed of the system allows a sharp detection of the edges of the fast moving piece of tape, while performing precise depth measurement of the four interfaces. Finally, in the fourth area marked by the blue arrow and presented in the inset, the metallic wire can be identified. Significantly, one can note that the 70 μm metallic wire, measured over a 2.4 μs range in the B-scan, contains 96 consecutive A-scans, indicating significant oversampling.

The experimentally implemented SS-OCT system presented in this article demonstrates the great potential of akinetic swept sources, and in particular, of those based on the method of spectrally broadened mode-locked lasers that use all-normal-dispersion supercontinuum dynamics. While this method is currently more expensive and bulkier compared to other solutions (FDML, MEMS-VECSEL), it presents flexibility in allowing to precisely target the A-scan rate, axial resolution or axial

range depending on the application. It is also, to the best of our knowledge, the only method to reach multiple tens of MHz A-scan rate at 1060 nm without any buffering.

Multiple possibilities can be investigated to overcome the current limitations. While a regenerative amplifier was needed in this case due to the low average power after stretching, new optical fibers with high normal dispersion can allow higher PSD. Additionally, alternative stretching methods such as chirped fiber Bragg gratings can give less loss than optical fiber at 1 μm and/or greater stretching which, combined with a lower repetition rate mode-locked laser, can give better sensitivity. Finally, further studies could benefit from a different interferometer design based on asymmetric configuration for better optical power management. The reasons above demonstrate high potential toward extending the capabilities of swept source technology.

IV. Conclusion

This paper reports a swept source based on a time-stretched, flat and smooth optical spectrum produced by ANDi supercontinuum generation processes. The source operates at 40 MHz with a bandwidth of 48.2 nm at FWHM, centered at 1060 nm. Using this laser, SS-OCT imaging at 40 MHz A-scan rate is demonstrated. The low noise of the source enables single-shot measurements with 12 μm axial resolution which, to the best of our knowledge, is the highest axial resolution achieved in the 1060 nm band with a MHz-rate akinetic swept-source. Imaging with the source is demonstrated using a fast moving object. This akinetic source demonstrates the validity of the approach for 1060 nm SS-OCT, and in future work, we aim to improve sensitivity and resolution to make the system more amenable for biomedical optics applications.

References

[1] Y. Li, J. Chen, and Z. Chen, "Advances in Doppler optical coherence tomography and angiography," *Transl. Biophotonics*, vol. 1, Nov. 2019, Art. no. e201900005.

[2] W. Wieser, B. R. Biedermann, T. Klein, C. M. Eigenwillig, and R. Huber, "Multi-megahertz OCT: High quality 3-D imaging at 20 million A-scans and 4.5 GVoxels per second," *Opt. Exp.*, vol. 18, no. 14, pp. 14685–14704, Jul. 2010.

[3] A. Y. Alibhai, C. Or, and A. J. Witkin, "Swept source optical coherence tomography: A review," *Curr. Ophthalmol. Rep.*, vol. 6, pp. 7–16, Mar. 2018.

[4] E. Moult et al., "Ultrahigh-speed swept-source OCT angiography in exudative AMD," *Ophthalmic Surg. Lasers Imag. Retina*, vol. 45, pp. 496–505, Nov. 2014.

[5] T. Klein and R. Huber, "High-speed OCT light sources and systems," *Biomed. Opt. Exp.*, vol. 8, no. 2, pp. 828–859, Feb. 2017.

[6] D. Huang, F. Li, Z. He, Z. Cheng, C. Shang, and P. K. A. Wai, "400 MHz ultrafast optical coherence tomography," *Opt. Lett.*, vol. 45, pp. 6675–6678, Dec. 2020.

[7] T. Klein, W. Wieser, L. Reznicek, A. Neubauer, A. Kampik, and R. Huber, "Multi-MHz retinal OCT," *Biomed. Opt. Exp.*, vol. 4, pp. 1890–1908, Oct. 2013.

[8] D. Huang, Y. Shi, F. Li, and P. K. Wai, "Fourier domain mode locked laser and its applications," *Sensors*, vol. 22, May. 2022, Art. no. 3145.

[9] J. Zhang et al., "Multi-MHz MEMS-VCSEL swept-source optical coherence tomography for endoscopic structural and angiographic imaging with miniaturized brushless motor probes," *Biomed. Opt. Exp.*, vol. 12, pp. 2384–2403, Apr. 2021.

[10] S. Moon and D. Y. Kim, "Ultra-high-speed optical coherence tomography with a stretched pulse supercontinuum source," *Opt. Exp.*, vol. 14, pp. 11575–11584, Nov. 2006.

[11] A. Mahjoubfar, D. V. Churkin, S. Barland, N. Broderick, S. K. Turitsyn, and B. Jalali, "Time stretch and its applications," *Nature Photon.*, vol. 11, no. 6, pp. 341–351, Jun. 2017.

[12] D. Huang, F. Li, C. Shang, Z. Cheng, and P. K. A. Wai, "Reconfigurable time-stretched swept laser source with up to 100 MHz sweep rate, 100 nm bandwidth, and 100 mm OCT imaging range," *Photon. Res.*, vol. 8, pp. 1360–1367, Aug. 2020.

[13] J. Xu, C. Zhang, J. Xu, K. K. Y. Wong, and K. K. Tsia, "Megahertz all-optical swept-source optical coherence tomography based on broadband amplified optical time-stretch," *Opt. Lett.*, vol. 39, pp. 622–625, 2014.

[14] J. Kang, P. Feng, X. Wei, E. Y. Lam, K. K. Tsia, and K. K. Y. Wong, "102-nm, 44.5-MHz inertial-free swept source by mode-locked fiber laser and time stretch technique for optical coherence tomography," *Opt. Exp.*, vol. 26, no. 4, pp. 4370–4381, 2018.

[15] X. Wei, C. Kong, G. K. Samanta, K. K. Tsia, and K. K. Y. Wong, "Self-healing highly-chirped fiber laser at 1.0 μm," *Opt. Exp.*, vol. 24, pp. 27577–27586, Nov. 2016.

[16] E. Genier, P. Bowen, T. Sylvestre, J. M. Dudley, P. M. Moselund, and O. Bang, "Amplitude noise and coherence degradation of femtosecond supercontinuum generation in all-normal-dispersion fibers," *JOSA B*, vol. 36, pp. A161–A167, 2019.

[17] M. Klimczak, B. Siwicki, A. Heidt, and R. Buczyński, "Coherent supercontinuum generation in soft glass photonic crystal fibers," *Photon. Res.*, vol. 5, no. 6, pp. 710–727, Dec. 2017.

[18] S. R. DS et al., "Shot-noise limited, supercontinuum-based optical coherence tomography," *Light: Sci. Appl.*, vol. 10, no. 1, pp. 1–13, Jun. 2021.

[19] A. M. Heidt et al., "Low noise all-fiber amplification of a coherent supercontinuum at 2 μm and its limits imposed by polarization noise," *Sci. Rep.*, vol. 10, no. 1, pp. 1–9, Oct. 2020.

[20] T. Sylvestre et al., "Recent advances in supercontinuum generation in specialty optical fibers," *JOSA B*, vol. 38, no. 12, pp. F90–F103, Dec. 2021.

[21] E. Genier et al., "Ultra-flat, low-noise, and linearly polarized fiber supercontinuum source covering 670–1390 nm," *Opt. Lett.*, vol. 46, no. 8, pp. 1820–1823, Apr. 2021.

[22] I. B. Gonzalo, R. D. Engelsholm, M. P. Sørensen, and O. Bang, "Polarization noise places severe constraints on coherence of all-normal dispersion femtosecond supercontinuum generation," *Sci. Rep.*, vol. 8, pp. 1–13, Dec. 2018.

[23] C. Finot, B. Kibler, L. Provost, and S. Wabnitz, "Beneficial impact of wave-breaking for coherent continuum formation in normally dispersive nonlinear fibers," *JOSA B*, vol. 25, pp. 1938–1948, Nov. 2008.

[24] J. M. Dudley, G. Genty, and S. Coen, "Supercontinuum generation in photonic crystal fiber," *Rev. Modern Phys.*, vol. 78, pp. 1135–1184, Oct. 2006.

[25] R. D. Engelsholm, "Low noise supercontinuum lasers for optical coherence tomography systems," Ph.D. dissertation, Tech. Univ. Denmark, 2018.

[26] S. Gupta and B. Jalali, "Time-warp correction and calibration in photonic time-stretch analog-to-digital converter," *Opt. Lett.*, vol. 33, no. 22, pp. 2674–2676, Nov. 2008.

[27] C. M. Eigenwillig, B. R. Biedermann, G. Palte, and R. Huber, "K-space linear fourier domain mode locked laser and applications for optical coherence tomography," *Opt. Exp.*, vol. 16, no. 12, pp. 8916–8937, Jun. 2008.

[28] S. Rivet, M. Maria, A. Bradu, T. Feuchter, L. Leick, and A. Podoleanu, "Complex master slave interferometry," *Opt. Exp.*, vol. 24, no. 3, pp. 2885–2904, Feb. 2016.

[29] A. Bradu et al., "Recovering distance information in spectral domain interferometry," *Sci. Rep.*, vol. 8, pp. 1–16, Dec. 2018.

[30] M. Jensen et al., "Noise of supercontinuum sources in spectral domain optical coherence tomography," *J. Opt. Soc. Amer. B*, vol. 36, pp. A154–A160, Feb. 2019.

[31] C. C. Rosa and A. G. Podoleanu, "Limitation of the achievable signal-to-noise ratio in optical coherence tomography due to mismatch of the balanced receiver," *Appl. Opt.*, vol. 43, no. 25, pp. 4802–4815, Sep. 2004.

[32] W. Drexler and J. G. Fujimoto, *Optical Coherence Tomography: Technology and Applications*. Berlin, Germany: Springer, Jan. 2015.

[33] A. F. Runge, C. Aguergaray, N. G. Broderick, and M. Erkintalo, "Coherence and shot-to-shot spectral fluctuations in noise-like ultrafast fiber lasers," *Opt. Lett.*, vol. 38, no. 21, pp. 4327–4330, Nov. 2013.